Supplement of Biogeosciences, 22, 181–212, 2025
https://doi.org/10.5194/bg-22-181-2025-supplement

Biogeosciences Open Access EGU

Supplement of

Development of the DO_3SE-Crop model to assess ozone effects on crop phenology, biomass, and yield

Pritha Pande et al.

Correspondence to: Pritha Pande (pritha.pande@york.ac.uk)

S1a. Resistance and diffusivity of gases across leaf boundary layers

The leaf-level quasi laminar boundary layer resistance term r_b (McNaughton and van der Hurk, 1995) incorporates empirically derived constants for heat and gas conductance (see Table S1, in mol TLA m^{-2} s^{-1}), cross-wind leaf dimension L (given in m) and the wind speed at the leaf surface $u(h)$ (given in m/s). N.B. TLA is Total Leaf Area.

Table S1. Empirically derived constant conductance (mol TLA m^{-2} s^{-1}) (and resistance (PLA s/m)) values for heat and gas (H_2O, CO_2 and O_3) from a single leaf surface.

Matter	**Conductance (mol TLA m^{-2} s^{-1})**	**Resistance (PLA s/m)** Rounded down
Heat	0.135	150
Water vapour, H_2O	0.147	139
Carbon dioxide, CO_2	0.110	186
Ozone, O_3	0.105	195

*N.B. The conversion of constants from conductance to resistance is achieved by multiplying by 2 to convert from single surface to PLA, dividing by 41 to convert from mol m^{-2} s^{-1} to m/s, and calculating the reciprocal to give a resistance term (e.g. for heat the conversion is 1/(0.135*2)/41 which gives 151.85 and is then rounded down to 150).*

Leaf boundary layer resistance for heat (for forced convection) $(r_{b,heat})$ can be calculated according to eq. [S1] after (Campbell, G.S., Norman, 1998), using the 150 value for boundary layer resistance to heat in s/m, these formulations take into account both sides of the leaf and therefore provide $r_{b,heat}$ for PLA (Projected Leaf Area)).

$$r_{bheat_{forced}} = 150.\sqrt{\frac{L}{u(h)}} \quad [S1]$$

To estimate boundary layer resistance values for other gases simply substitute the relevant gas constant for resistance into eq. [S1].

S1b. Diffusivities of gases for stomatal conductance

The conversion factors are derived from Graham's law which assumes that the ratio of the diffusivities is equal to the inverse of the square root of the ratio of molecular weights (as described in (Campbell, G.S., Norman, 1998)).

e.g. mol H_2O m^{-2} s^{-1} = 0.61 mol O_3 m^{-2} s^{-1}

mol CO_2 m^{-2} s^{-1} = 0.96 mol O_3 m^{-2} s^{-1}

	Molecular weight	Ratio of molecular weights (to H_2O)	Ratio of molecular weights (to CO_2)	Ratio of molecular weights (to O_3)	Inverse sq. root of ratio of molecular weight (to H_2O)	Inverse sq. root of ratio of molecular weight (to CO_2)	Inverse sq. root of ratio of molecular weight (to O_3)

H_2O	18	1	0.409	0.375	1	1.56	1.63
CO_2	44	2.44	1	0.92	0.64	1	1.04
O_3	48	2.67	1.09	1	0.61	0.96	1

S2. Irradiance absorption by the canopy

Solar radiation is the key determinant of the productivity of any crop. The radiation absorbed (direct and diffuse) photosynthetically active radiation, PAR_{tot} (in W/m^2)) by crops will have a direct impact on canopy photosynthesis (and associated stomatal conductance) and affect crop leaf phenology and hence net primary productivity (NPP). PAR absorbed by crops is divided into two categories, direct (PAR_{dir}) and diffuse (PAR_{diff}) radiation. PAR_{dir} is the PAR which reaches the crop leaf surface without being scattered, whereas PAR_{diff} can be naturally (by cloud cover and naturally occurring particles in the atmosphere) or artificially scattered (e.g. by pollutant aerosol). PAR can also be reflected by surfaces.

To estimate the total irradiance (PAR_{tot} which is equal to PAR_{dir} + PAR_{diff}) incident on sunlit and shaded parts of the canopy we use the method of (De Pury and Farquhar, 1997).

S2a.Total Photosynthetic Active Radiation (PAR_{tot})

PAR absorbed per unit leaf area is divided into PAR_{dir}, PAR_{diff} which also includes scattered (re-reflected by the canopy) beam calculated by,

$$PAR_{dir}\,(LAI) = (1 - \rho_{cb}(\beta))\; k_b{}'\; I_b(0)\; exp(-k_b{}'LAI) \quad \text{[S1]}$$

Where, $\rho_{cb}(\beta) = 1 - \exp\left[\frac{2\rho_h\, k_b}{1+k_b}\right]$ [S2]

$K_b{}'$is beam and scattered beam PAR extinction coefficient; $I_b(0)$ is the initial beam irradiance, representing the intensity of direct sunlight before it interacts with the canopy

$$PAR_{diff}\,(LAI) = \;(1 - \rho_{cd})\; k_d{}'\; I_d(0)\; exp(-k_d{}'LAI) \quad \text{[S3]}$$

Where; $\rho_{cd} = \frac{1}{I_d\,(0)} \int_0^{\frac{\pi}{2}} N_d\;(\alpha)\rho_{cb}\,(\alpha)d\alpha$ [S4]

K_d' is diffuse and scattered diffuse PAR extinction coefficient

The total absorbed irradiance per unit leaf area is calculated as:

$$PAR_{total} = \; PAR_{dir}\,(LAI) \; + \; PAR_{diff} \;\text{(LAI)} \quad \text{[S5]}$$

Estimations of the direct, diffuse and scattered (re-reflected) irradiance are necessary to calculate the *PAR* incident on the sunlit (*LAI*$_{sun}$) and shaded (*LAI*$_{sh}$) portions of the canopy, which are then calculated based on the equations described below:

S2b. Total irradiance absorbed as shaded leaves ($I_{lsh}\,(LAI)$)per unit leaf area are calculated as;

$$PAR_{sh}(LAI) \; = \; PAR_{diff}(LAI) \; + \; PAR_{bs}(LAI) \quad \text{[S6]}$$

where $PAR_{diff}(LAI)$ is diffuse irradiance (see eq.) and $PAR_{bs}(LAI)$, direct scattered beam (another form of diffuse radiation) is calculated as:

$$PAR_{bs}(LAI) \; = \; PAR_b\;(0)\;[\,PAR_{dir} - (1 - \;\sigma)k_b exp(-k_b LAI)\} \quad \text{[S7]}$$

S2c. Total irradiance absorbed by per unit leaf area of the sunlit leaf

$$PAR_{sun}\,(LAI,\beta) = PAR_{sh}\,(LAI) + PAR_{bsun}\,(\beta) \quad [S8]$$

Where; $PAR_{sh}\,(LAI)$ is irradiance absorbed by shaded leaves (see equation S7) and $PAR_{bsun}\,(\beta)$, beam irradiance absorbed by sunlit leaves and calculated as below:

$$PAR_{bsun}\,(\beta), = (1 - \sigma)I_b(0)\frac{Cos_{\alpha l}}{Sin\beta} \quad [S9]$$

S3. Solar elevation Angle

sinβ which is defined as the solar elevation angle, varies over the course of the day as a function of latitude and day length as described in eq. 8, this eq. and the other solar geometry equations required for its calculation are taken from Campbell & Norman, (1998).

$$\sin\beta = \sin\lambda\,.\,\sin\delta + \cos\lambda\,.\cos\delta\,.\cos hr \quad [S10]$$

where β is the solar elevation above the horizontal, λ is the latitude, δ is the angle between the sun's rays and the equatorial plane of the earth (solar declination), *hr* is the hour angle of the sun and is given by $[15(t\text{-}t0)]$ where *t* is time and t_o is the time at solar noon.

The solar declination (δ) is calculated according to eq. 9.

$$\delta = -23.4cos\,[360(td + 10)/365] \quad [S11]$$

where t_d is the year day.

The time, *t* is in hours (standard local time), ranging from 0 to 23. Solar noon (t_o) varies during the year by an amount that is given by the equation of time (*e*, in min) and calculated by:

$$t_o = 12 - LC - e \quad [S12]$$

where *LC* is the longitude correction. *LC* is + 4 or –4 minutes for each degree you are either east or west of the standard meridian. *e* is a 15 to 20-minute correction, which depends on the year day according to eq. S13.

$$e = \frac{-104.7\sin f + 596.2\sin 2f + 4.3\sin 3f - 12.7\sin 4f - 429.3\cos f - 2.0\cos 2f + 19.3f}{3600} \quad [S13]$$

where $f = 279.575 + 0.9856\,t_d$ in degrees.

It is also necessary to calculate the day length so that the hour angle of the sun can be calculated throughout the day. Day length is defined as the number of hours that the sun is above the horizon and requires the hour angle of the sun, *hr*, at sunrise or sunset to be calculated with eq. S14.

$$cos\,hr = -tan\lambda.tan\delta \quad [S14]$$

so that day length in hours equals $2hr/15$.

S4. Methodology for gap-filling and standardisation of data for AgMIP Ozone

This document describes the methodological approach that was applied in order to search for gaps and quality issues in time-series (gas concentration and meteorological) datasets, and the approach used for filling gaps.

Where gaps had already been filled by the team collecting the data then this interpolated data was left under the assumption that it would be a more accurate reflection of the experimental conditions.

Gap filling methodology for hourly data: During the data standardisation process some data gaps were identified. These ranged in size from a single hour of missing data to several consecutive hours, to several consecutive days, weeks, or even months. A requirement of input data for modellers is that it is continuous; the following gap filling methodology was therefore devised. These gap filling methods are only applied for the duration of the plants growing season (i.e. between sowing and harvest):

Single hours of missing data were filled by taking the average of the hourly values coming the hour before, and the hour after, the missing value.

Several consecutive hours of missing data (23 hours or less) were filled by taking the average of the corresponding hour the day before, and the day after; and repeating this for each missing hour of data. If data were unavailable from that hour of the previous day, then only the value from the day after was used and vice versa. If there is no data available in either the day before or after, then the method is used (see below point 2.).

Gaps larger than 24 hours could be filled using the following methods:

1. Gaps between 24 hours and 168 hours (i.e. from 1 day up to 1 week) would be filled with the averages from that same hour of the equivalent day, the week before and the week after (i.e. averaging 2 numbers). If data were unavailable from those hours of the previous week, then only the values from the week after would be used (and vice versa).
2. Gaps longer than 1 week would be filled with the diurnal averages from one week before and after the period of missing data (i.e. potentially averaging 14 hours of data, but in cases where data is sparse then it could only be a couple of hours). Gap filled values would not be used in calculating averages. Where data is daily, i.e. some meteorological data, the average of the 7 days before and/or after is used.

There were some instances where data gaps extended for several months. For these extensive gaps, the following methods were used:

All datasets from Xiaoji, China, had about a 4-month gap in meteorological and ozone data at the start of the growing season. At this stage of the growing season, plants will either have not yet emerged or have a very small LAI and therefore any ozone uptake would have been minimal. Ozone gaps were filled with the diurnal averages of the first two weeks of the ambient experimental data for each year. Meteorological data was filled using Nasa Power data (https://power.larc.nasa.gov/data-access-viewer/). The variables selected are in the appendix below. In Xiaoji China, global radiation was measured, whereas the Nasa Power data platform only provides Photosynthetically Active Radiation (PAR). To convert global

radiation to PAR, values were multiplied by two and divided by 24 to be comparable with global radiation in MJ/m2/hour.

If the gap occurs before exposure data begins then the ambient or non-filtered treatment is gap filled using the above methodology and then this data is used for all treatments to ensure that concentrations are not overestimated. If there is no ambient treatment, then averages of the treatment closest to ambient is used. If there are gaps in gas data after the beginning of exposure date, then averages from that treatment are used (as opposed to ambient). If no date for start of exposure is provided, then exposure is assumed to start when the gas data begins (even if it is na). Similarly, once exposure has ended then only averages from the period after exposure were used. If there was not enough data to base averages on, then ambient data was used (Nottingham 1996).

Any ozone values of less than 0 were treated as gaps and filled following the above methods, depending on the size of gap.

If mean air temperature was not available but minimum and maximum air temperature was, the average of these two values was used and the source of the data was label 'c' for calculated.

Sections of the dataset which had been gap filled were clearly identified using a categorisation system in an adjacent 'data source' column, so that these data could be identified at a later stage, and so that alternative measured or modelled data could be sought. The percentage of gap-filled data within the total time-series for each gas concentration and meteorological variable was also reported in the readme file accompanying each dataset.

The Parameters downloaded from (https://power.larc.nasa.gov/data-access-viewer/) Hourly data was downloaded from the Nasa Power data access viewer for Xiaoji, China to fill gaps in meteorological data. The following parameters were selected: 1. Agroclimatology community; 2. Hourly; 3. Lat/long: 32.58333: 119.7; 4. Time extent: Determined by data gap in each year; 5. Format: CSV format; 6. Parameters: a) temp at 2m, b)relative humidity at 2m, c)wind speed at 2m, d) precipitation, e) radiation: "All Sky Surface photosynthetically active radiation" (PAR Total) (MJ/m^2/day). This was converted to hourly global radiation (MJ/m2/h) by dividing to 24 and multiplying with 2 because PAR ~ 0.5 * global radiation

S5. O_3 Resistance

Atmospheric Resistance

$$r_a = \frac{1}{K\,u^*}\left(\log\left(\frac{z_2}{z_1}\right) - \Psi_h\left(\frac{z_2}{L}\right) + \Psi_h\left(\frac{z_1}{L}\right)\right)$$

u^* Friction velocity m/s

K Von Karman's constant

L Monin-Obukhov length m

z_1 Lower height m

z_2 Upper height m

Ψ_h Flux-gradient stability function for heat

Heat flux

$$\Psi_h(x) = \begin{cases} 2\log\left(\frac{1+\sqrt{1-16x}}{2}\right) & x < 0 \\ -5x & x \geq 0 \end{cases}$$

Quasi-laminar boundary layer resistance

$$r_{b,O3} = \frac{2}{Ku^*}\left(\frac{\left(\frac{V}{diff}\right)}{PR}\right)^{\frac{2}{3}}$$

u^* Friction velocity m/s

K Von Karman's constant

V Kinematic viscosity of air at 20°C m^2/s

$diff$ Molecular diffusivity in air m^2/s

PR Prandtl number

In-canopy resistance

$$r_{inc} = 14\frac{SAI\ h}{u^*}$$

External plant cuticle resistance

$$r_{ext} = \frac{2500}{SAI}$$

Stomatal resistance

$$r_{sto} = \min\left(100000, \frac{41000}{g_{sto}}\right)$$

Surface resistance per layer

$$r_c = \begin{cases} r_b + \frac{1}{\left(\frac{1}{r_{sto}} + \frac{1}{r_{ext}}\right)} & LAI > 0 \\ r_b + r_{ext} & SAI > 0 \end{cases}$$

S6. Analysis of RYL estimates

We find that we tend to underestimate the O_3-induced relative yield loss (RYL) by between -2.76 and 15.34 (observed less modelled RYL) across all years and cultivars. Tables S3a and S3b show that average differences between observed and modelled RYL estimates for all cultivars are similar between years (ranging from 4.94 to 6.73) but that average differences between cultivars across years are more variable with the sensitive cultivars (Y2 and Y19) ranging between 5.02 and 9.0; and

tolerant cultivars (Y16 and Y15) ranging between 2.66 and 5.54. This would suggest that O_3-induced RYLs can be more reliably modelled for tolerant cultivars which may suggest that additional processes causing O_3-induced yield losses in sensitive cultivars are not captured by the model, such as O_3 altering the allocation of C to different plant parts (Feng et al., 2008) or O_3 inducing additional respiratory costs *via* the upregulation of defence mechanisms (Biswas et al., 2008).

Table S2a. Comparison of O_3-induced relative yield loss (RYL) between observed and modelled by year and cultivar. Also shown is the difference (Observed – Modelled) in RYL.

Year	Cultivar, Type	RYL (Observed)	RYL (Modelled)	Difference RYL (Observed – Modelled)
2007	Y2, Sensitive	25.58	16.23	9.35
2008	Y2, Sensitive	23.82	19.36	4.46
2009	Y2, Sensitive	26.15	12.82	13.33
2007	Y2, Sensitive	18.72	16.23	2.49
2008	Y19, Sensitive	34.70	19.36	15.34
2009	Y19, Sensitive	10.06	12.82	-2.76
2007	Y16, Tolerant	19.51	13.29	6.22
2008	Y16, Tolerant	16.69	14.22	2.47
2009	Y16, Tolerant	19.37	11.44	7.93
2007	Y15, Tolerant	15.37	13.29	2.08
2008	Y15, Tolerant	18.88	14.22	4.66
2009	Y15, Tolerant	12.70	11.44	1.26

Table S2b. Average differences (Observed – Modelled) in O_3-induced relative yield loss (RYL) between observed and modelled grouped by years and cultivars. Also shown is the difference in RYL for the training dataset.

	Average Relative Yield Loss
Y2, Sensitive (all years)	9.05
Y19, Sensitive (all years)	5.02
Y16, Tolerant (all years)	5.54
Y15, Tolerant (all years)	2.67
2007 (all cultivars)	5.04
2008 (all cultivars)	6.73
2009 (all cultivars)	4.94
Y2, Y16, 2008 (training data)	3.47

Fig S1. The Chinese FACE-O3 dataset were used to plot modelled phenological stages against experimental dataset for the year 2008 (training set)

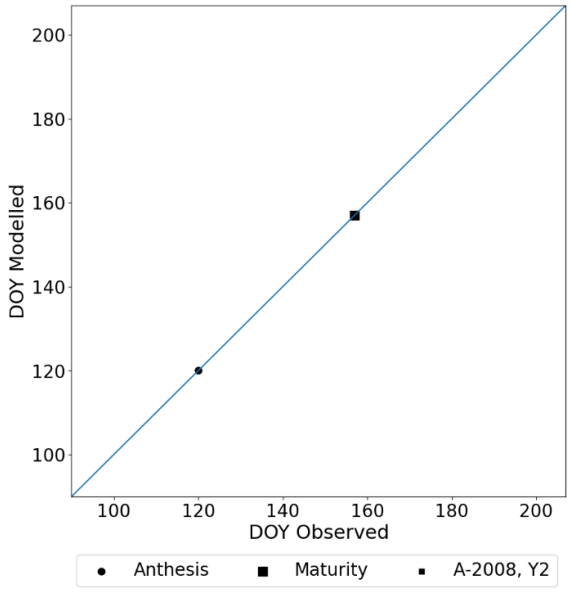

Fig S2. The Chinese FACE-O3 datasets were used to plot DO3SE-crop LAI (m^2/ m^2) against the observed dataset for the years a.) 2007 and b.) 2008 for the ambient O_3 treatments.

a).

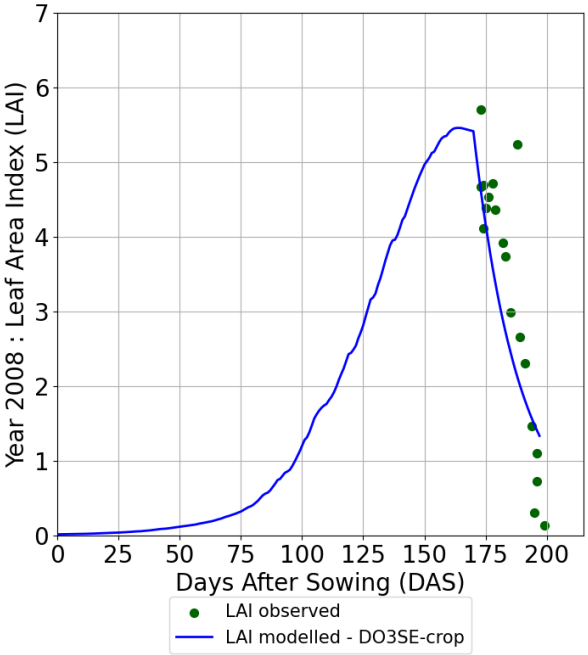

b).

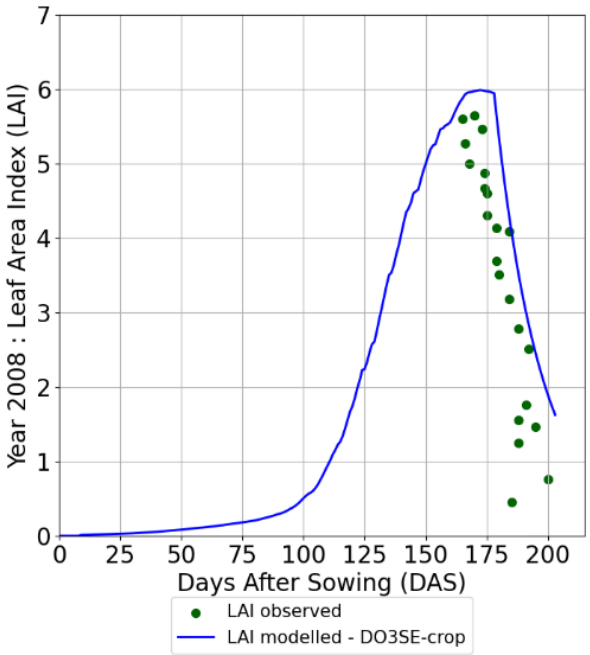

Fig S3. The Chinese FACE-O3 dataset were used to plot modelled grain dry matter (g/m^2) against the experimental dataset for the year 2008 for tolerant (Y16) and sensitive cultivar (Y2) (training set)

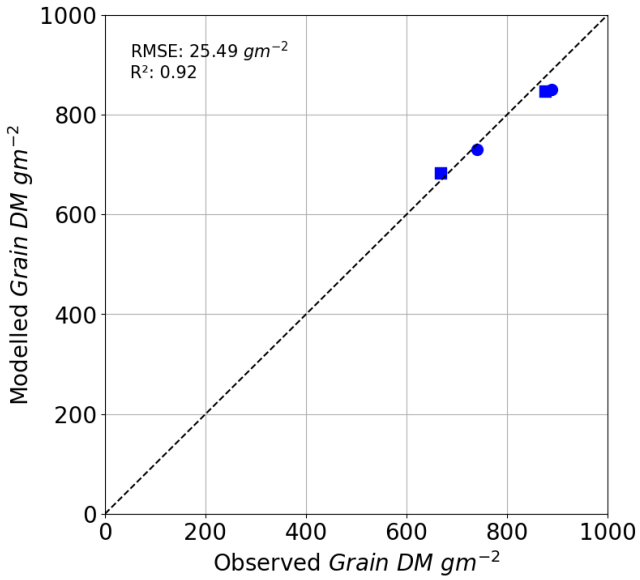

Fig S4. Profiles of O_3 induced leaf senescence for the Y2 cultivar for the a). AA O_3 treatment and b). E O_3 treatment. The timing of the SOS (solid black line) and EOS (dashed black line) were determined by applying the break point method to the chlorophyll data and are shown in relation to the f_{LS} simulations of senescence (yellow solid line). The observed normalised chlorophyll content data, shown as filled blue symbols, include error bars representing the standard deviation of the measurements.

a).

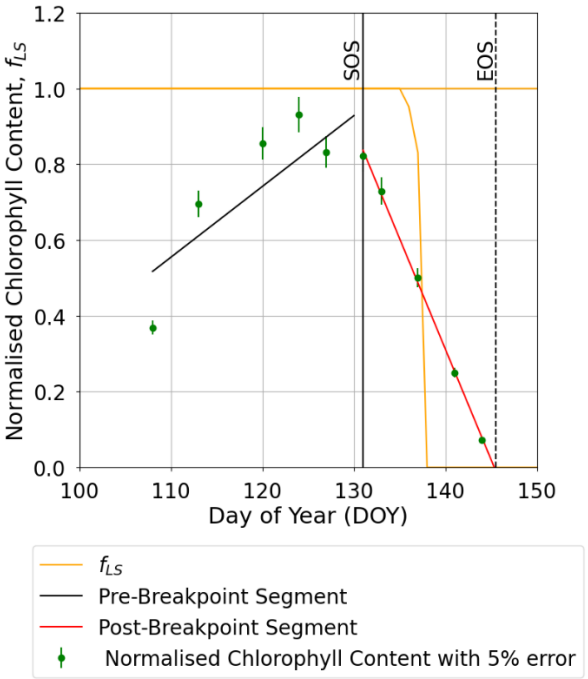

b).

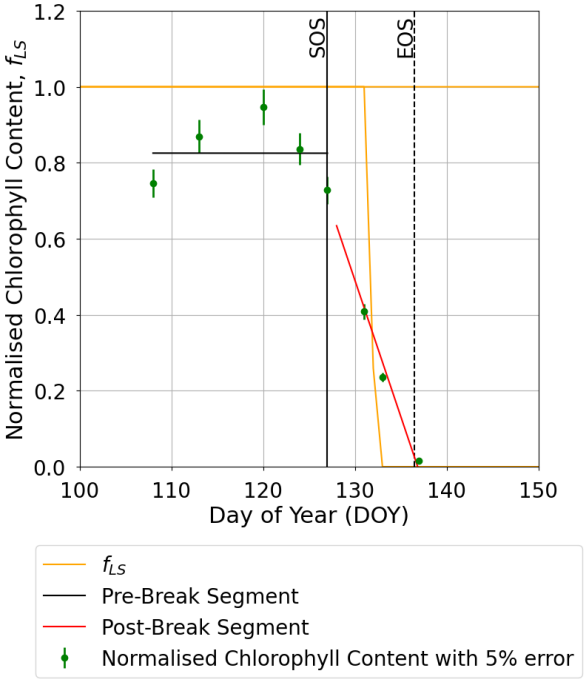

Fig S5. Comparison of daily maxima seasonal profiles of DO_3SE-Crop modelled canopy leaf vs observed flag leaf data for a). AA O_3 treatment A_{net}, and b). AA O_3 treatment g_{O3} and c) E O_3 treatment A_{net}, and d). E O_3 treatment g_{O3} for the period from the anthesis (i.e., TT_{rep}) for the year 2008 and the Y2 cultivar. The left (solid blue line) and right (solid red line) represent the segment fits to the normalised chlorophyll content values for application of the breakpoint method to define the SOS (Start of Senescence) shown as the solid black dashed line. The green scatter solid dots, along with their standard measurement error, represent the normalised observed chlorophyll content values (see Fig S4 for further details).

a).

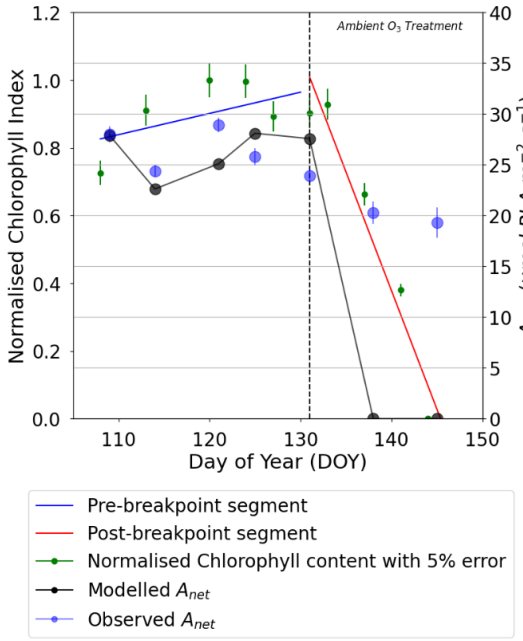

b).

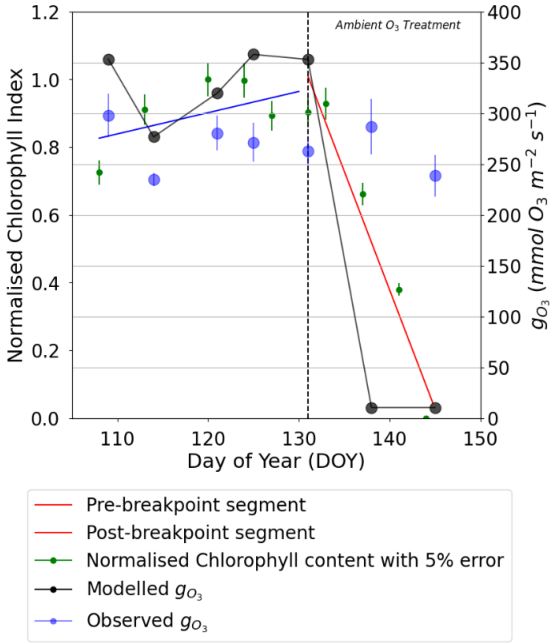

c).

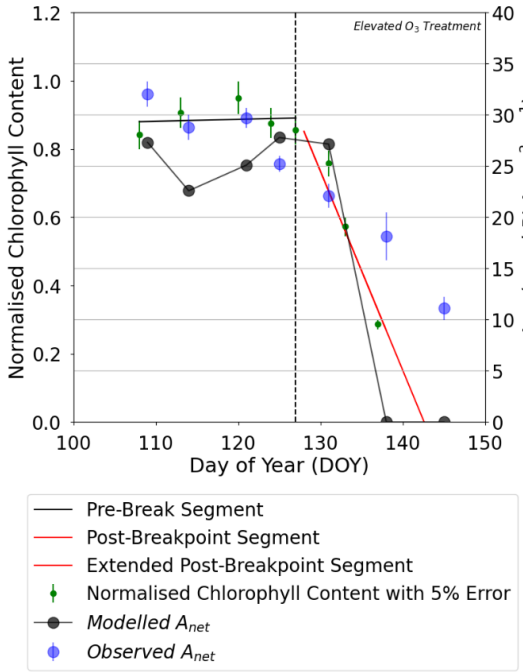

d).

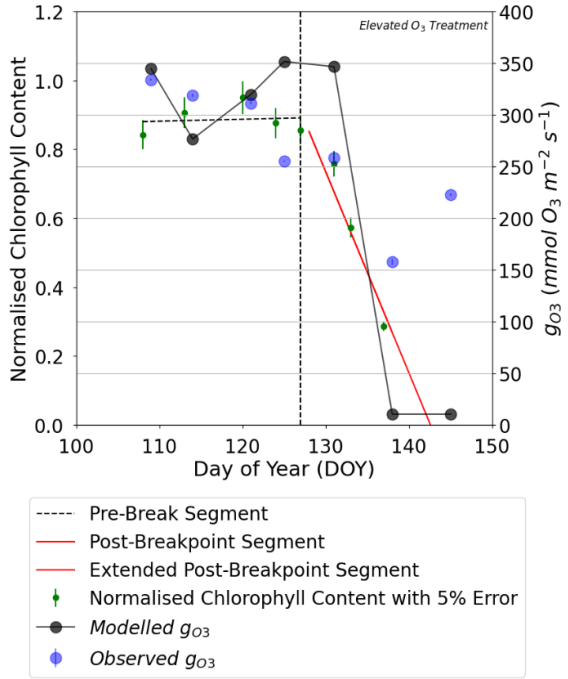

Table S5. The table describes the calibration and evaluation steps for the DO_3SE-crop model and the datasets used in each step.

Calibration step	**Approach**	**Parameters Identified/included/evaluated**	**Years/cultivars/treatments**
1	Sensitivity analysis to identify key parameters for calibration for crop growth and yield	leaf photosynthesis parameters: V_{cmax25}, J_{max25}, kN, m, VPD_0; C allocation parameters: α_{root}, α_{leaf}, α_{stem}, Υ , τ, R_{dcoeff}, R_{gcoeff}	2008, Y2, AA
2i	Automated calibration of phenology module using genetic algorithm	Phenology parameters: T_b, T_0, T_m, VT_{min}, VT_{max}, PIV, and PID, TT_{emr}, TT_{veg}, TT_{rep}, and T_l	2008, Y2 & Y16, AA
2ii	Manual calibration of leaf physiology	Leaf photosynthesis parameters: V_{cmax25}, J_{max25}, kN, m, VPD_0	2008, Y2 & Y16, AA
2iii	Manual calibration of C allocation	C allocation parameters: α_{root}, α_{leaf}, α_{stem}, Υ , τ, R_{dcoeff}, R_{gcoeff}	2008, Y2 & Y16, AA
2iv	Manual calibration of O_3 damage	O_3 damage parameters: γ_3, γ_4 and γ_5, $CLsO3$	2008, Y2 & Y16, A and EO_3
3	Evaluation	$Grain\ DM$	2007, Y2, Y15, Y16, Y19, A and EO_3 2008, Y15, Y19, A and EO_3 2009, Y2, Y15, Y16, Y19, A and EO_3

Fig S6. Sensitivity analysis of different plant physiological parameters for two scenarios: S1 (baseline conditions) and ST (treatment conditions, such as ozone stress for this study). Panel (a) represents the sensitivity indices (S1, ST) for variables including (V_{cmax}, J_{max}, kN, m, and VPD_0) on critical physiological outputs such as g_{O3}, A_{net}, and $Grain\ DM$ Panel (b) shows sensitivity indices for other parameters (α_{root}, α_{leaf}, α_{stem}, β_{root}, β_{leaf}, β_{stem}, Υ affecting the same outputs

a).

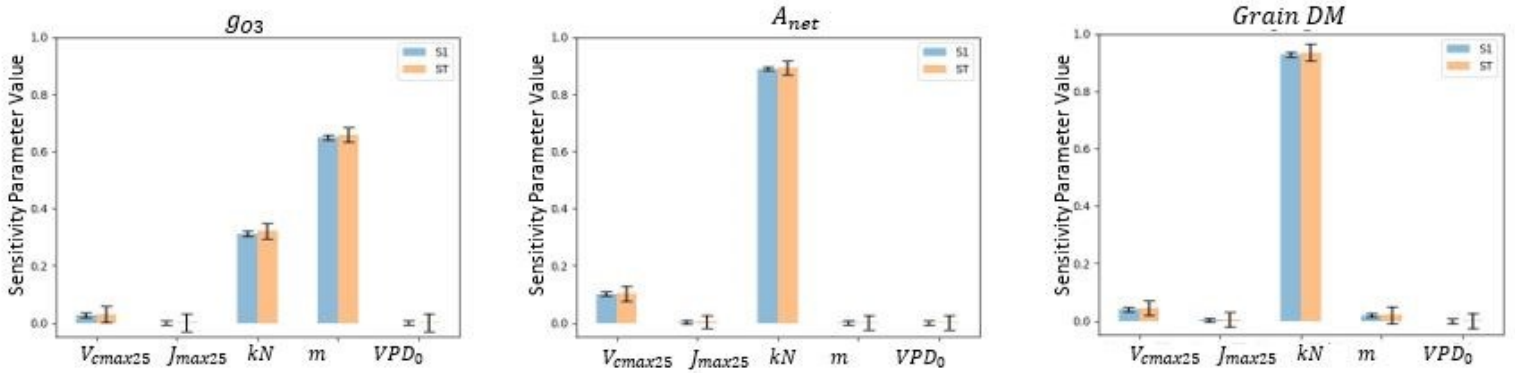

b).

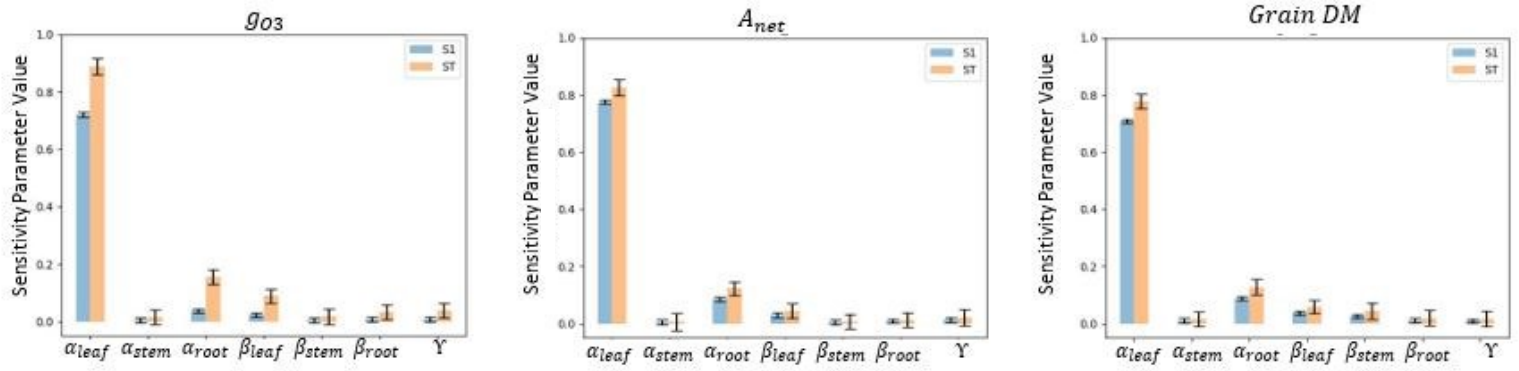

References :

Campbell, G. S., and Norman, J. M.: *An Introduction to Environmental Biophysics*, Second Edition, Springer, 1998.

De Pury, D. G. G., and Farquhar, G. D.: *Simple scaling of photosynthesis from leaves to canopies without the errors of big-leaf models*, Plant, Cell and Environment, 20, 537–557, https://doi.org/10.1111/j.1365-3040.1997.00094.x, 1997.

Biswas, D. K., Xu, H., Li, Y. G., Sun, J. Z., Wang, X. Z., Han, X. G., and Jiang, G. M.: *Genotypic differences in leaf biochemical, physiological and growth responses to ozone in 20 winter wheat cultivars released over the past 60 years*, Global Change Biology, 14, 2087–2098, https://doi.org/10.1111/j.1365-2486.2007.01477.x, 2007.

Büker, P., Emberson, L. D., Ashmore, M. R., Cambridge, H. M., Jacobs, C. M. J., Massman, W. J., Müller, J., Nikolov, N., Novak, K., Oksanen, E., Schaub, M., and de la Torre, D.: *DO3SE modelling of soil moisture to determine ozone flux to forest trees*, Atmospheric Chemistry and Physics, 12, 5537–5562, https://doi.org/10.5194/acp-12-5537-2012, 2012.

Clark, D. B., Mercado, L. M., Sitch, S., Jones, C. D., Gedney, N., Best, M. J., Pryor, M., Rooney, G. G., Essery, R. L. H., Blyth, E., Boucher, O., Harding, R. J., Huntingford, C., and Cox, P. M.: *The Joint UK Land Environment Simulator (JULES), model description – Part 2: Carbon fluxes and vegetation dynamics*, Geoscientific Model Development, 4, 701–722, https://doi.org/10.5194/gmd-4-701-2011, 2011.

Ewert, F., and Porter, J. R.: *Ozone effects on wheat in relation to CO2: Modelling short-term and long-term responses of leaf photosynthesis and leaf duration*, Global Change Biology, 6, 735–750, https://doi.org/10.1046/j.1365-2486.2000.00351.x, 2000.

Feng, Z., Kobayashi, K., and Ainsworth, E. A.: *Impact of elevated ozone concentration on growth, physiology, and yield of wheat (Triticum aestivum L.): a meta-analysis*, Global Change Biology, 14, 2696–2708, https://doi.org/10.1111/j.1365-2486.2008.01673.x, 2008.

Feng, Y., Nguyen, T. H., Alam, M. S., Emberson, L., Gaiser, T., Ewert, F., and Frei, M.: *Identifying and modelling key physiological traits that confer tolerance or sensitivity to ozone in winter wheat*, Environmental Pollution, 304, 119251, https://doi.org/10.1016/j.envpol.2022.119251, 2022.

Feng, Y., Wu, L. B., Autarmat, S., Alam, M., and Frei, M.: *Testing the responses of four wheat crop models to heat stress at anthesis and grain filling*, Global Change Biology, 22, 1890–1903, https://doi.org/10.1111/gcb.13212, 2016.

Lu, X., Zhang, L., Liu, Z., Gao, M., Zhao, Y., and Shao, J.: *Lower tropospheric ozone over India and its linkage to the South Asian monsoon*, Atmospheric Chemistry and Physics, 18, 3101–3118, https://doi.org/10.5194/acp-18-3101-2018, 2018.

Luo, Y., Zhang, Z., Chen, Y., Li, Z., and Tao, F.: Wang: *ChinaCropPhen1km: a high-resolution crop phenological dataset for three staple crops in China during 2000-2015 based on leaf area index (LAI) products*, Earth System Science Data, 12, 197–214, https://doi.org/10.5194/essd-12-197-2020, 2020.

Medlyn, B. E., Dreyer, E., Ellsworth, D., Forstreuter, M., Harley, P. C., Kirschbaum, M. U. F., Le Roux, X., Montpied, P., Strassemeyer, J., Walcroft, A., Wang, K., & Loustau, D.: *Temperature response of parameters of a biochemically based model of photosynthesis. II. A review of experimental data*, Plant, Cell and Environment, 25, 1167–1179, https://doi.org/10.1046/j.1365-3040.2002.00891.x, 2002.

Mulvaney, M. J., and Devkota, P. J.: *Adjusting Crop Yield to a Standard Moisture Content*, EDIS, 2020, https://doi.org/10.32473/edis-ag442-2020, 2020.

Osborne, S., Pandey, D., Mills, G., Hayes, F., Harmens, H., Gillies, D., Büker, P., & Emberson, L.: *New insights into leaf physiological responses to ozone for use in crop modelling*, Plants, 8, 84, https://doi.org/10.3390/plants8040084, 2019.

Osborne, T., Gornall, J., Hooker, J., Williams, K., Wiltshire, A., Betts, R., & Wheeler, T.: *JULES-crop: A parametrisation of crops in the Joint UK Land Environment Simulator*, Geoscientific Model Development, 8, 1139–1155, https://doi.org/10.5194/gmd-8-1139-2015, 2015.

Pande, P., Hayes, F., Bland, S., Booth, N., Pleijel, H., and Emberson, L. D.: *Ozone dose-response relationships for wheat can be derived using photosynthetic-based stomatal conductance models*, Agricultural and Forest Meteorology, 356, 110150, https://doi.org/10.1016/j.agrformet.2024.110150, 2024.

Sharkey, T. D., Bernacchi, C. J., Farquhar, G. D., and Singsaas, E. L.: *Fitting photosynthetic carbon dioxide response curves for C3 leaves*, Plant, Cell and Environment, 30, 1035–1040, https://doi.org/10.1111/j.1365-3040.2007.01710.x, 2007.

Tao, F., Zhang, S., and Zhang, Z.: *Spatiotemporal changes of wheat phenology in China under the effects of temperature, day length and cultivar thermal characteristics*, European Journal of Agronomy, 43, 201–212, https://doi.org/10.1016/j.eja.2012.07.005, 2012.

Wang, J., Wang, E., Feng, L., Yin, H., and Yu, W.: *Phenological trends of winter wheat in response to varietal and temperature changes in the North China Plain*, Field Crops Research, 144, 135–144, https://doi.org/10.1016/j.fcr.2012.12.020, 2013.

Zhao, H., Zheng, Y., Zhang, Y., and Li, T.: *Evaluating the effects of surface O3 on three main food crops across China during 2015–2018*, Environmental Pollution, 258, 113794, https://doi.org/10.1016/j.envpol.2019.113794, 2020.